Micro-electrode *in vivo* signatures of human periventricular heterotopia

Valerio Frazzini[1,2,*], Stephen Whitmarsh[2,*], Virginie Lambrecq[1,2], Katia Lehongre[2], Pierre Yger[3], Bertrand Mathon[4], Claude Adam[1], Dominique Hasboun[2,5], and Vincent Navarro[1,2,†]

[1]*AP-HP, Epilepsy Unit, Pitié-Salpêtrière Hospital and Sorbonne University, Paris, France*

[2]*ICM (Institute of Brain and Spinal Cord, INSERM UMRS1127, CNRS UMR7225, Sorbonne University), Pitié-Salpêtrière Hospital, Paris, France*

[3]*Sorbonne Université, INSERM, CNRS, Institut de la Vision, 17 rue Moreau, F-75012 Paris, France*

[4]*AP-HP, Department of Neurosurgery, Pitié-Salpêtrière Hospital and Sorbonne University, Paris, France*

[5]*AP-HP, Department of Neuroradiology, Pitié-Salpêtrière Hospital and Sorbonne Université, Paris, France*

[*] Contributed equally to this study.

†Corresponding author: Prof. Vincent Navarro, MD, PhD, Epileptology unit, Pitié-Salpêtrière Hospital, and Brain and Spine Institute (ICM; INSERM, CNRS, Sorbonne Université), 47 boulevard de l'Hôpital, 75651 Paris cedex 13, France; Tel: 33 1 42 16 19 40, Fax: 33 1 42 16 19 42; E-mail: vincent.navarro@aphp.fr

ORCID: Valerio Frazzini 0000-0003-1187-3352, Stephen Whitmarsh 0000-0002-3969-6565, Pierre Yger 0000-0003-1376-5240, Vincent Navarro 0000-0003-0077-8114

Abstract

Periventricular nodular heterotopia (PNH) is a common cause of drug-resistant epilepsy, characterized by nodules of ectopic neurons adjacent to the lateral ventricles. While ectopic neurons are suspected to be involved in epileptogenesis, their long-term in vivo recording in epileptic patients has so far been lacking. We report the first multi-level analysis of long-term microelectrode recordings from three nodules in two epileptic patients during presurgical evaluation. In both patients, seizures originated from the ectopic nodules. Highly consistent interictal activities were identified from microelectrodes: 1) trains of periodic slow waves , 2) isolated slow deflections, both with superimposed fast activity , and 3) epileptic spikes. Patterns were highly local and largely invisible on the adjacent macro-electrode contacts. Extracellular action potential analyses showed that the majority of units were strongly modulated during all interictal patterns. We further identified, for each individual neuron, different types of firing rate modulation, corresponding to the different interictal patterns. These results are consistent with an altered regulation of cellular excitability and suggest that periodic patterns may result from fluctuation in inhibition and rebound excitation in the same neuronal network.

1 Introduction

Periventricular nodular heterotopia (PNH) is one of the most common types of cortical malformation (Guerrini & Dobyns, 2014). PNH is the result of an abnormal neuronal migration process wherein clusters of ectopic neurons form nodular masses of gray matter close to the walls of the lateral ventricles (Dubeau et al., 1995). The majority of patients with PNH suffer from focal pharmaco-resistant epilepsy (Battaglia et al., 2006) for which neurosurgery can be considered. Stereotaxic EEG (SEEG) is often required for pre-surgical evaluation of the seizure onset zone (SOZ), as seizures might start in PNH, overlying cortex, or both (Stefan et al., 2007; Aghakhani, 2005; Battaglia et al., 2006; Francione et al., 1994; Kothare et al., 1998; Tassi, 2004; Valton et al., 2008).

The SOZ can also be inferred from patterns of interictal activity that are known to correlate with specific epileptogenic lesions. For example, patients with type-IIb focal cortical dysplasia frequently show localized periodic or pseudo-periodic spikes or poly-spikes (Palmini et al., 1995). In PNH, reports of stereotypical interictal patters are more limited. One sEEG study found an absence of background activity in PNH, together with low voltage, low frequency activity, frequent high voltage spikes and positive waves (Tassi, 2004), while another study only reported frequent low voltage spikes-and-waves (Mirandola et al., 2017). Neurons within the ectopic tissue are disorganized (Dubeau et al., 1995), which would limit spatial summation of electric currents and might contribute to the heterogeneity in sEEG findings. Microelectrodes, however, can record local-field-potentials (LFPs) and spikes from nearby ($\approx 140\,\mu m$) neurons, and are therefor less dependent on the spatial summation of current flow (Buzsáki, 2004). Furthermore, recording spike activity from PNH can evaluate unequivocally the involvement of ectopic neurons rather than surrounding tissues in epileptic activities.

The goal of our study was to identify and then investigate interictal LFP patterns that originate locally within the epileptogenic nodules in PNH, using micro-electrodes. Secondly, we investigated whether these LFP patterns correspond to modulation of neuronal firing rates in PNH. Lastly, combining several parameters, we tried to investigate whether the detected units were associated with different cell categories. For these purposes, interictal patterns were described on an unprecedented level of microscopic detail by means of microelectrode recordings from three PNH nodules in two patients. LFP patterns were initially identified on the basis of their morphological and pathological features and the described in the time- and frequency domain. Single units were extracted using spike-sorting algorithms (Yger et al., 2018), after which extracellular spike-width and peak-trough time were used to describe units on the basis of detected morphological and electrophysiological features (Henze et al., 2000).

2 Materials and method

2.1 sEEG recording

Two patients were implanted with bilateral intracranial depth electrodes (AdTech®). Two (Patient 1) and three (Patient 2) Behnke-Fried type macro-micro electrodes were inserted. Platinum macroelectrode contacts were separated by 5 mm (⌀= 1.3 mm). These electrodes included eight microelectrodes and one reference wire (≈ 2 mm long, ⌀=40 µm) extending from the tip of the electrode shaft and able to record non-overlapping cell populations (Fried et al., 1999). Trajectories, anatomical targets, number of electrodes and number of electrode contacts, were determined according to the clinical practice and the epilepsy features of the patients. Implantation was performed at the Department of Neurosurgery of the Pitié-Salpêtrière Hospital using Leksell frame-based stereotaxy (Patient 1) or using the robotic assistant device ROSA (ROSA® Brain, Medtech, France; Patient 2). Signals from macro- and microelectrodes were continuously and synchronously recorded at 4 kHz and 32 kHz, respectively, using a hardware filter at 0.01 Hz (Atlas Recording System; NeuraLynx, Tucson, AZ, USA). Post-implantation electrode locations were based on pre-implantation 3 T 3D-MRI, post-implant 1.5 T 3D-MRI and CT scan, integrated using the Epiloc toolbox, an in-house developed plugin for the 3D-Slicer visualization software (Fedorov et al., 2012). Following implantation, patients were continuously monitored for seizures in the Epilepsy Unit (16 days for patient 1 and 20 days for patient 2), after which the SOZ was determined by trained clinical neurophysiologists. All macroelectrodes had at least one verified contact in the PNH (Table 2). The patients gave a written informed consent (project C11-16 conducted by INSERM and approved by the local ethic committee, CPP Paris VI).

2.2 Visual analysis of micro-LFP patterns

Pathological patterns recorded by the micro-electrodes were identified according to traditional morphological characteristics used in clinical practice (Gotman & Gloor, 1976). Criteria for each pattern were then determined and used for a complete manual scoring of continuous data recorded at the first day after implantation. Patient 1 was analyzed for 24 hours, while Patient 2, due to richness of interictal activity, was analyzed for 6 hours. Annotation of data was performed with software developed in-house (MUSE), using single markers for epileptic spikes, and start/end-markers for prolonged patterns and artefacts. To determine duration and periodicity of the patterns, onset and duration of every deflection were also determined manually on a subset of patterns. In case of periodic patterns, only sequences with at least 3 consecutive deflections were included. Periodicity was determined in accordance with Hirsch et al. (2013), by calculating the percentage of deflections that deviated more than 25% from the average period within each pattern.

2.3 Spectral analysis of micro-LFP patterns

Analyses were performed with a combination of FieldTrip (Oostenveld, Fries, Maris, & Schoffelen, 2011) and custom MATLAB scripts (The Mathworks Inc., Natick, Massachusetts). Time-courses were first aligned according to the max/min peak of (the envelope of) filtered data (Supplementary Table 1). Data was then down-sampled to 1 kHz. Average LFPs were based on the aligned time-courses. Time–frequency representations (TFRs) were calculated using a Hanning taper applied to an adaptive sliding time window of seven cycles ($t = 7/f$, $\Delta t = 10\,\text{ms}$). Average power in 10 Hz-200 Hz was then expressed in percentage change, relative to the baseline-period at -2 s to -1 s relative to pattern onset. For epileptic spikes a baseline period of -1 s to -0.5 s was used, except for the second nodule of Patient 2, where a baseline-period of -2 s to -1 s was used due to more extended fluctuations of firing rate preceding the epileptic spike.

2.4 Spike sorting and analysis

After selecting clean electrodes, data was temporally whitened, and spikes were automatically detected at 6 median absolute deviations of high-pass filtered ($> 500\,\text{Hz}$) data. Spikes that occurred during artefacted periods were ignored. A combination of density-based clustering and template matching algorithms were used to automatically cluster the detected spikes (Yger et al., 2018). Clusters that were not stable across the whole recording were discarded from further analysis. Clusters were further evaluated whether they reflected putative single-unit activity (SUA) or multi-unit activity (MUA) based on ISI (inter-spike-interval), the percentage of refractory period violation ($RPV = ISI < 21\,\text{ms}$) and spike morphology. Resting behaviour of detected units were further explored by mean firing rate, Fano factor % CV, (Shinomoto, Shima, & Tanji, 2003) and bursting index (BI) (Constantinidis & Goldman-Rakic, 2002), based on the baseline period preceding epileptic spikes to maximize the number of events. Spike-times were epoched and time-locked identically to the LFP analyses. Average spike rates were calculated continuously at 1000 Hz, using a Gaussian smoothing kernel of 12.5 ms for Epileptic Spikes, and 50 ms for the longer patterns to investigate the slower modulation in firing rate. Correlations between average time-locked spike-rates of each unit, and the average time-locked LFP of every pattern, were calculated. Finally, spike-rates of each trial were binned into 200-bins for statistical analyses. To control for multiple comparisons and non-normal distributions of firing-rates, we performed non-parametric cluster-based permutation tests (Maris & Oostenveld, 2007) to determine time-periods where firing-rates changed significantly from baseline. A threshold of $p < 0.01$ (first-level t-test) was used to determine contiguous clusters, after which a threshold of $p < 0.05$ (one-sided) determined whether the clusters (sum of t-values) could be explained under permutation ($n = 1000$). Finally, an exploratory classification of single units into putative pyramidal and interneurons, was based on half-width

duration and trough-peak time of their waveforms (Barthó et al., 2004).

3 Results

3.1 Novel LFP epileptic activity revealed by microelectrodes

In both patients, seizures started at electrode contacts located in the PNH, with a secondary propagation in other cortical areas (Fig 1J,K & Supplementary clinical info). Importantly, we identified striking interictal activities of which three main interictal patterns were found to be consistent over nodules (Fig 1 & 2). These patterns were rarely visible on the macro-electrodes. Furthermore, epoch-by-epoch correlations between the microelectrode and adjacent macroelectrode contacts showed that the interictal patterns were restricted to the PNHs (Fig. 2E).

3.1.1 Periodic Slow Waves

Nodule 1 and Nodule 2 displayed Periodic Slow Waves (PSW; Fig 1C&F). The periodicity of the PSW was clear in the average LFP of Nodule 1 (Fig 2A, right) and Nodule 2 (Fig 2B, right). Average ($\pm\sigma$) duration of a single slow wave was 283 ± 74 ms in Nodule 1, and 271 ± 72 ms in Nodule 2. Time periods between onset of two slow waves was 511 ± 148 ms in Nodule 1, and 574 ± 152 ms in Nodule 2. 83% (Nodule 1, $n = 181$) and 79% (Nodule 2, $n = 153$) of these time periods varied less than 25% from the average period; therefore these events occurred periodically *periodic* (Hirsch et al., 2013). Low voltage fast activity (FA) was superimposed on the slow waves. (Fig 1C&F). Frequency analysis showed a mean peak at 112 Hz (Nodule 1) and 137 Hz (Nodule 2). These FA were clearly modulated in accordance with the periodicity of the slow waves.

3.1.2 Fast Activity

In Nodule 1 and 2, microelectrode recordings showed *isolated* trains of FA. In Nodule 1, FA was usually superimposed on a polyphasic slow deflection (0.5 s-1 s, Fig 1C, middle), while in Nodule 2, FA occurred at the onset of a sharply appearing slow deflection (2 s-4 s, Fig 1F, middle). Time-frequency analysis showed that in Nodule 1, power increased 43 Hz and 96 Hz for ≈ 0.5 s. Nodule 2 showed a clear narrow-band increase of power at 112 Hz for at least 1 s. Those events were isolated, with no tendency to ictal organisation. In Nodule 3, low amplitude deflections coincided with periodic short trains of fast activity, that lasted for 326 ± 79 ms. Periods were 1075 ± 241 ms (Fig. 1F). 91% of the periods varied less than 25% ($n = 155$) from the average period, in accordance with a definition of *periodic* (Hirsch et al., 2013). Time-frequency analysis showed clear periodic modulation of high frequency power, centered on 110 Hz (Fig 2D, right).

3.1.3 Epileptic Spikes

Epileptic Spikes (ES) were identified in all three nodules. Specifically, Nodule 1 showed isolated sharp monophasic waves (Fig 1C, left). In Nodule 2, spikes were generally followed (and often preceded) by a slow wave (Fig 1F, left), which is shown in the average (Fig 2B, left). In Nodule 3, spikes were characterized by a low amplitude di- or triphasic wave (Fig 1I, left). Low voltage FA were superimposed on ES, measured by time frequency analysis at 113Hz, 137Hz and 126Hz, respectively, and time-locked to the ES.

3.2 Massive neuronal recruitment by interictal patterns

Twenty-one microelectrodes were included in the analysis (Nodule 1: n=6, Nodule 2: n=7, Nodule 3: n=8). Spike clustering resulted in 25 units (Table 1, Fig 4A) of which 8 (32%) were classified as single units. Single units were shown to significantly modulate their firing rates in response to all interictal patterns. Firing-rate increased up to 505% for PSW, 4281% for FA, and 3840% for ES (Table 1: ↑). Most of the units also showed brief episodes of decreased firing rate surrounding the interictal activities, often by $\approx$ 100% to near silence (Table 1: ↓), Fig 2 and Fig 3A-C). Furthermore, trial-by-trial correlations showed that the modulation of firing rates were highly consistent with the timing and shape of the interictal LFP in all units, showing strongly significant correlations between firing rates and interictal LFPs for all units (Table 1 see also: Fig. 2, Fig. 3A-C). A massive increase of firing rate were shown for the very short duration of the ES, while FA was associated with more prolonged increase of firing rate. During PSW, firing rates showed regular increases and decreases of firing rate. Interestingly, three clusters, including 2 putative single units, significantly modulated their firing-rate in inversely to interictal LFPs (Fig 2C, Table 1: Nodule 2, Unit 4&5; Nodule 3, Unit 2).

3.3 Exploratory classification of neuronal types

An exploratory classification of single units into neuronal types was done by means of clustering based on the half-width and trough-to-peak time of the action-potential (Fig 4A). Values separating the two clusters of putative inter-neurons (Fig 4A, left panel: pyramidal cells in top-right, interneurons in bottom-left) were consistent with previous reports (Trough-to-peak: ≈ 0.5 ms, Half-amplitude duration: ≈ 0.25 ms (Barthó et al., 2004)). Out of the 8 units detected, 7 were classified as putative pyramidal cells (example waveform Fig 4A: inverted pyramid, while one was consistent with a narrow-spiking putative interneuron (waveform Fig 4A: star). No clear differences were observed in mean firing rate over trials (FR), CV or Burst Index, but the interneuron did show the highest Fano Factor of all cluster (Fig 4B).

4 Discussion

Chronically implanted microelectrodes revealed highly local interictal and ictal events in human PNH. Three distinct interictal LFP patterns were identified: Periodic Slow Waves with Fast Activity (PSW+FA), isolated slow wave with Fast Activity (FA), and epileptic spikes (ES). Except for the latter, none of these LFP patterns have ever been described before, and this study therefore provides a potentially highly selective neurophysiological marker of PNH. Duration and periodicity of these uncovered interictal patterns were consistent features across the patients and nodules, while time-locked averaging further confirmed a consistent morphology. Spectral analyses showed that these interictal patterns were associated with sustained periods of high frequency activity (110 Hz-137 Hz), further emphasizing their pathological nature.

Spike analysis revealed a massive recruitment of PNH neurons during the interictal activities. The large majority of the units strongly modulates their firing rate according to *all* interictal LFP patterns. These striking findings are in line with a hyper-synchronous and hyper-excitable neuronal population, consistent with the emerging understanding of the pathophysiology of PNH. Heterotopic neurons have been found to be more excitable as result of a deficient A-type potassium currents (Castro, Cooper, Lowenstein, & Baraban, 2001), while NR2A and NR2B subunit expression and regulatory molecular machinery are reduced in preclinical rat models (Colacitti et al., 1999) and, importantly, in resected human PNH tissue (Finardi et al., 2006). Moreover, a previous *in vitro* study found a dramatic increase in inhibitory GABAergic synaptic transmission of heterotopic neurons, which could reflect a compensating drive against the otherwise hyper-excitability of the pathological network of PNH (Calcagnotto, Paredes, & Baraban, 2002; Kitaura et al., 2012).

Two findings provide further insights into the question of why, and how, these different LFP patterns were generated. First , as the majority of units strongly responded to all interictal patterns, and none showing a clear preference for one pattern over another, we can speculate that the interictal patterns were generated by the same neuronal population. Second, differences in modulation of the firing rate surrounding the time of interictal discharges, suggest that specific network conditions might determine which interictal pattern will occur. Our data shows that during the isolated trains of FA the increase in firing rate was more sustained than in the other patterns, while periods of suppression preceding the pattern were more inconstant. In contrast, epileptic spikes (ES) were associated with shorter increase in firing rate and were clearly preceded and followed by a strong synchronous decrease in firing rate across all clusters, within a time-frame of 500 ms. Taken together, we could make the following hypotheses. First, periodic patterns may result from alternating inhibition and rebound excitation in the same neuronal network. Second, different dynamics of the rebound excitation result in different LFP patterns. Specifically, epileptic spikes could be

caused by highly synchronous, transient rebounds in firing rate, whereas long duration slow wave activity could be caused by a more asynchronous rebound resulting in prolonged cycles of alternating inhibition and excitation.

An exploratory analysis suggests that both putative pyramidal cells and interneurons were recovered, in accordance with histological studies showing both excitatory neurons and interneurons in human PNH (Thom, Martinian, Parnavelas, & Sisodiya, 2004; Meroni et al., 2009). However, neuronal types did not distinguish between interictal patterns, neither could we conclude any different behaviour correlated with their classification.

This study presents the first *in vivo* multi-level description of local PNH networks in humans and their organization into multiple epileptic neurophysiological patterns. Previous micro electrode studies showed strong heterogeneity in neuronal firing during cortical and mesial temporal interictal discharges(Keller et al., 2010; Le Van Quyen et al., 2008; Alvarado-Rojas et al., 2013). In contrary, we found that most units were recruited in interictal patterns, showing consistent firing among each pattern. This difference might have resulted from the fact that our recording was highly local and only included PNH tissue, while the previous study analyzed several cortical regions and cerebral lesions. More research is needed to further elucidate the neuronal mechanism underlying interictal activity in PNH, including the question why some neurons modulated their firing rate in anti-correlation with the LFP, and whether these interictal patterns can be found in sub-cortical heterotopia or other malformations arising from an abnormal migrational process.

5 Figures

		Macro plot							
N	Micro	1	2	3	4	5	6	7	8
1^R	GM PNH	GM PNH	GM PNH lat	GM STS	GM STS	GM STS	GM SMG	GM SMG	XC
2^R	GM PNH	GM PNH	GM PNH lat	WM	GM STG	GM STS^{T2}	GM STS^{T2}	GM^{T2}	GM^{T2}
3^L	GM PNH	GM PNH im	GM PNH im	LTO	LTO^{T3}	WM	WM	GM/WM^{T3}	GM^{T3}

Table 1: Localization of electrode contacts. N = Nodule, L = Left, R = Right hemisphere, PNH = Periventricular Heterotopic Nodule, GM = Grey matter, WM = White matter, lat = lateral, im = inferior medial, LTO = Lateral, Temporo-Occipital Sulcus, SMG = SupraMarginal Gyrus, STS = Superior Temporal Sulcus, T2 = Middle Temporal Gyrus, T3 = Inferior Temporal Gyrus.

N	ID	#	RPV	ES ↑	ES ↓	ES ρ	FA ↑	FA ↓	FA ρ	PSW ↑	PSW ↓	PSW ρ	F2
1	2	35402	0.09	$3840^{\ddagger}$	$95^{\ddagger}$	$0.68^{\ddagger}$	$406^{\ddagger}$	$83^{\ddagger}$	$0.63^{\ddagger}$	$355^{\ddagger}$	$82^{\ddagger}$	$0.79^{\ddagger}$	A
	7	35603	0.03	$285^{\ddagger}$	$98^{\ddagger}$	$0.50^{\ddagger}$	$493^{\ddagger}$	$69^{\ddagger}$	$0.68^{\ddagger}$	$128^{\ddagger}$	$76^{\ddagger}$	$0.70^{\ddagger}$	
	1	324414	3.32	$373^{\ddagger}$	$69^{\ddagger}$	$0.74^{\ddagger}$	$319^{\ddagger}$	$48^{\ddagger}$	$0.54^{\ddagger}$	$153^{\ddagger}$	$54^{\ddagger}$	$0.84^{\ddagger}$	
	3	59035	0.77	$2421^{\ddagger}$	$84^{\ddagger}$	$0.66^{\ddagger}$	$238^{\ddagger}$	$58^{\ddagger}$	$0.60^{\ddagger}$	$180^{\ddagger}$	$71^{\ddagger}$	$0.82^{\ddagger}$	
	4	9032	0.43	$3074^{\ddagger}$	$100^{\ddagger}$	$0.75^{\ddagger}$	$361^{\dagger}$	$96^{\dagger}$	$0.47^{\ddagger}$	$201^{\ddagger}$	$81^{\ddagger}$	$0.80^{\ddagger}$	
	5	75177	1.48	$1575^{\ddagger}$	$65^{\ddagger}$	$0.90^{\ddagger}$	$249^{\ddagger}$	$63^{\ddagger}$	$0.54^{\ddagger}$	$305^{\ddagger}$	$61^{\ddagger}$	$0.88^{\ddagger}$	
	6	28386	0.72	$1144^{\ddagger}$	$97^{\ddagger}$	$0.72^{\ddagger}$	$468^{\ddagger}$	$79^{\ddagger}$	$0.69^{\ddagger}$	$216^{\ddagger}$	$66^{\ddagger}$	$0.66^{\ddagger}$	
2	5	177686	0.90	$24^{\ddagger}$	$91^{\ddagger}$	$-0.45^{\ddagger}$	n.s.	$93^{\ddagger}$	$-0.68^{\ddagger}$	$22^{\ddagger}$	$26^{\ddagger}$	$-0.68^{\ddagger}$	C
	8	22797	0.67	$1582^{\ddagger}$	$97^{\ddagger}$	$0.67^{\ddagger}$	$4281^{\ddagger}$	100^{*}	$0.86^{\ddagger}$	$505^{\ddagger}$	$98^{\ddagger}$	$0.83^{\ddagger}$	
	1	6523	0.14	$524^{\ddagger}$	$100^{\ddagger}$	$0.44^{\ddagger}$	n.s.	n.s.	$0.07^{\ddagger}$	$170^{\ddagger}$	n.s.	$0.43^{\ddagger}$	
	2	11431	0.45	$599^{\ddagger}$	$96^{\ddagger}$	$0.45^{\ddagger}$	n.s.	$100^{\dagger}$	$0.09^{\ddagger}$	$105^{\ddagger}$	60^{*}	$0.39^{\ddagger}$	
	3	92917	1.78	$1058^{\ddagger}$	$99^{\ddagger}$	$0.59^{\ddagger}$	$646^{\ddagger}$	$100^{\ddagger}$	$0.53^{\ddagger}$	$392^{\ddagger}$	$91^{\ddagger}$	$0.56^{\ddagger}$	
	4	20365	0.56	n.s.	$60^{\ddagger}$	$-0.16^{\ddagger}$	n.s.	$100^{\ddagger}$	$-0.29^{\ddagger}$	n.s.	n.s.	$-0.26^{\ddagger}$	
	6	56998	0.57	$40^{\ddagger}$	$52^{\ddagger}$	$0.28^{\ddagger}$	n.s.	n.s.	n.s	n.s.	n.s.	$0.24^{\ddagger}$	
	7	15479	2.47	$900^{\ddagger}$	$89^{\ddagger}$	$0.71^{\ddagger}$	$1536^{\ddagger}$	$100^{\dagger}$	$0.85^{\ddagger}$	$231^{\ddagger}$	$60^{\ddagger}$	$0.75^{\ddagger}$	B
	9	79082	3.36	$744^{\ddagger}$	$97^{\ddagger}$	$0.80^{\ddagger}$	$1484^{\ddagger}$	$100^{\ddagger}$	$0.69^{\ddagger}$	$264^{\ddagger}$	$87^{\ddagger}$	$0.74^{\ddagger}$	
	10	156754	2.52	$153^{\ddagger}$	$78^{\ddagger}$	$0.64^{\ddagger}$	$118^{\ddagger}$	$73^{\dagger}$	$0.49^{\ddagger}$	$35^{\dagger}$	$39^{\ddagger}$	$0.44^{\ddagger}$	
3	2	24774	0.48	$1905^{\ddagger}$	$100^{\ddagger}$	$-0.12^{\ddagger}$	$297^{\ddagger}$	$98^{\ddagger}$	$0.70^{\ddagger}$	-	-	-	
	4	5020	0.02	n.s.	$100^{\ddagger}$	$0.39^{\ddagger}$	588^{*}	$100^{\ddagger}$	$0.65^{\ddagger}$	-	-	-	
	5	4429	0.00	1968^{*}	$100^{\ddagger}$	$0.49^{\ddagger}$	467^{*}	$100^{\ddagger}$	$0.66^{\ddagger}$	-	-	-	
	7	13844	0.14	1825^{*}	$100^{\ddagger}$	0.05^{*}	$543^{\ddagger}$	$100^{\ddagger}$	$0.67^{\ddagger}$	-	-	-	D
	1	103242	3.87	$1796^{\ddagger}$	$96^{\ddagger}$	$0.36^{\ddagger}$	$181^{\ddagger}$	$91^{\ddagger}$	$0.74^{\ddagger}$	-	-	-	
	3	43938	1.33	$1153^{\ddagger}$	$99^{\ddagger}$	$0.37^{\ddagger}$	$291^{\ddagger}$	$93^{\ddagger}$	$0.50^{\ddagger}$	-	-	-	
	6	23329	0.90	$1042^{\ddagger}$	$94^{\ddagger}$	$0.26^{\ddagger}$	$267^{\ddagger}$	$78^{\ddagger}$	$0.78^{\ddagger}$	-	-	-	
	8	11527	0.65	1232^{*}	$100^{\ddagger}$	0.05^{*}	$465^{\ddagger}$	$100^{\ddagger}$	$0.75^{\ddagger}$	-	-	-	

Table 2: Spike analysis summary. N = Nodule, ID = unit, # = number of axion potentials, ES = Epileptic spike, FA = fast activity, PSW = periodic slow wave (for Nodule 3, Periodic Fast Activity is placed under FA for convenience). Increases (↑) and decreases (↓) in % firing-rate of baseline for most significant temporal cluster (n.s. = non significant), ρ = Pearson correlation between spikerate and LFP. Superscript symbols denote statistical significance ($* = p < 0.025$, $\dagger = p < 0.01$, $\ddagger = p < 0.001$). F2 = Panel of Figure 2 for more detailed presentation. Single units highlighted in gray.

6 Acknowledgements

We would like to thanks Pierre Pouget (ICM, Salpêtrière hospital, Paris, France) for the helpful discussion on the first draft of the manuscript.

7 Funding

This study was supported by the program "Investissements d'avenir" ANR-10-IAIHU-06, and grants from the OCIRP-ICM and the Fondation de l'APHP pour la Recherche - Marie-Laure PLV Merchandising.

8 Competing interests

The authors report no competing interests.

9 Supplementary material

Patient description

Patient 1

Patient 1 was investigated for refractory seizures starting at the age of 20. In the beginning, ictal symptoms were characterized by the appearance of vertigo and nausea followed by vocalizations, gestural and alimentary automatisms with loss of consciousness. Reported seizures had an average duration of 1-2 minutes. The patient had at least 20-25 seizures per month and no focal to bilateral tonic-clonic seizures were reported. At the moment of hospitalization the patient was on Lamotrigine 300 mg/day, Lacosamide 350 mg/day, Carbamazepine 800mg/day, Clobazam 15 mg/day. Previous used anti-epileptic drugs (AEDs) without efficacy were Valproate, Levetiracetam and Zonisamide. Brain MRI showed a PNH located in the temporal horn of the right ventricle associated with dysplastic overlying cortex. During the long-term scalp video-EEG recording, interictal activity consisted of focal, intermittent slowing in the right posterior temporal region associated with abundant epileptic spikes and sharp waves, diffusing also in the right anterior temporal regions. Recorded seizures began with fast rhythmic activity in the right temporal region then diffed into bilateral frontal regions, but with a predominance of the right hemisphere. Surprisingly, the interictal 18FDG-PET scan demonstrated subcortical hyper-metabolism most prominent in the nodular heterotopia. For the purpose of pre-surgical evaluation, 8 intracerebral electrodes were placed in the right posterior temporal region in order study the cortical malformation during three weeks of continuous recording. Several spontaneous seizures were detected, usually recorded first from electrodes located into the posterior aspects of the PNH. On the basis of the spread of the epileptic activity to other structures of the epileptic network, seizures could be associated to different clinical symptoms. When seizures were restricted to the nodule and nearby cerebral structures, clinical symptoms were usually characterized by the appearance of vertigo. When discharges were longer in duration and showed wider cerebral diffusion, the most common associated clinical symptoms were staring, loss of consciousness and motor automatisms. Sometimes seizures reoccurred within very short intervals, behaving as bursts of epileptic discharges. In this case, symptomatology was reported to be characterized by short episodes of loss of awareness. Seizures were electrically characterized by the appearance of slow deflection overlapped with fast rhythms between 115Hz and 160Hz, starting from the posterior part of PNH (Fig 1J). Further evidence for the nodule region as putative epileptic zone (EZ) was gained by means of electrical stimulation of the posterior portion of the nodule, which promoted the appearance of symptoms described by the patient as typical ictal clinical manifestation (dizziness). In contrast, electrodes located into the hippocampal regions and the anterior aspects of the nodule were not found

to participate in seizure initiation. More than 50 ictal discharges were found during the 16 days recording period.

Patient 2

Patient 2 was affected by a focal epilepsy since the age of 25. She experienced two main types of seizures. The first one was characterized by the appearance of a tingling sensation of the trunk and the head lasting few seconds, followed by loss of consciousness. During these seizures, the patient no longer understood what was said, and could not speak or read, although she may still perceived and heard what was happening around her. She also experienced a rapid successions of memories, thoughts, déjà vu, sweating and sometimes had to vomit. Autonomic symptoms were sometimes followed by visual manifestations of retinal persistence and dysmorphopsia. She presented post-critical dysphasia that could last for tens of minutes. A second type of seizure consisted of hot flashes, tachycardia and "short disconnection", that lasted for a few seconds. No secondary focal to bilateral seizures were reported. The patient reported at least one seizure per day. Surface EEG recordings found abundant interictal epileptic abnormalities represented by short bursts of spikes or spike and waves in the left posterior temporal or temporo-occipital regions. Sporadic spikes were found in the right frontal or temporal region during sleep. Ictal EEG was characterized by the appearance of rhythmic activity in left posterior temporal region showing some diffusion in the in the contro-lateral hemisphere. Brain MRI revealed bilateral periventricular heterotopies, predominantly in the posterior regions, with no morphological or signal abnormalities of adjacent cortical or hippocampal structures. Interictal PET found that PHNs were isometabolic with the overlying cortex, while the ictal SPECT detected a hypermetabolic aspect of the left temporal, central and posterior cortical areas, but not relevant ictal metabolic modifications in the PNH. At time of presurgical evaluation, she was on Lamotrigine 400 mg/day. Previous essayed treatments are Oxcarbamazepine, Pregabalin, Lacosamide and Topiramate. The patient was implanted with 8 deep electrodes investigating the temporo-parietal junctions bilaterally together with the underlying PHNs. Detected interictal abnormalities were most prominent during sleep and were represented by epileptic spikes arising from the left posterior nodules then diffusing to the temporal cortex and by large spikes from the left hippocampus (Fig 1K). Several asymptomatic seizures were detected during sleep, starting as a low voltage fast activity arising from plots located the left heterotopic nodules (were microelectrodes were also located, see Table 2). Longer seizures were usually associated with appearance of subtle motor signs such and sniffles. Electrically, those seizures began with a fast rhythmic activity evolving in the form of large spike-wave discharges detected in the left posterior nodules. On the contrary, diurnal seizures were usually symptomatic, consisting of tingling sensations of shoulders and trunk, remounting to the head, sometimes

followed by forced head rotation to the right, eyelids blinking, small vocalizations and blowing. At least 25 ictal discharges were recorded during 20 days of recording. Seizures originated mainly from the left nodules, with the anterior compartment initially most involved in the development of seizures.

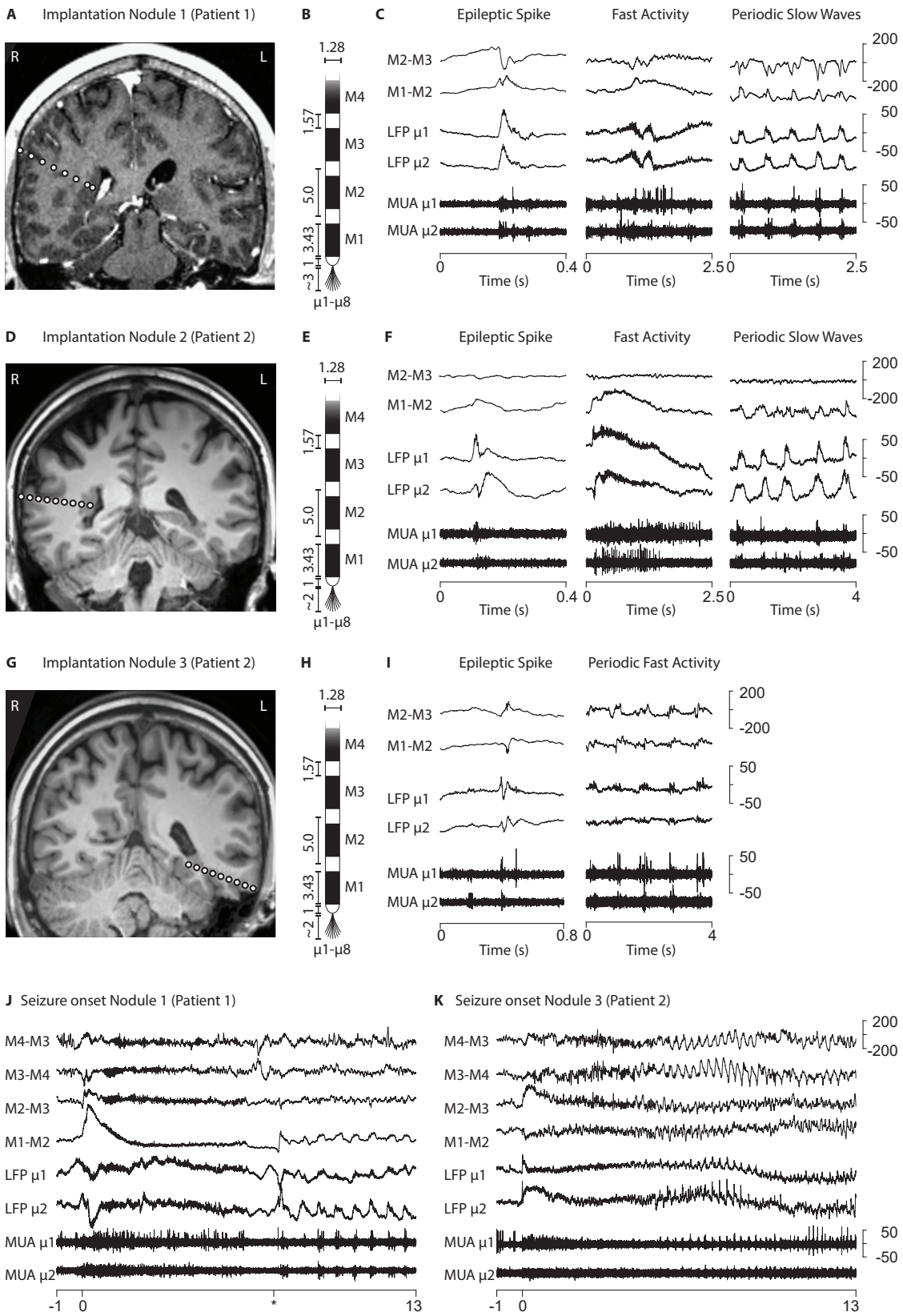

Figure 1: Patient implantation and their LFP patterns (continued on next page)

Figure 1: (A) Patient 1 was implanted with a macro-micro electrode (B) in a right periventricular nodule. Three LFP patterns were recorded, apparent on microelectrodes, and to a smaller degree on macroelectrodes (C). LFP patterns were associated with MUA recorded on the microelectrodes. (D) Patient 2 was implanted with bilateral macro-micro electrodes (E,H) into periventricular nodules. Similar patterns as in Patient 2 were apparent on the micro LFP, and to a smaller degree on macro LFPs (F,I). LFP patterns were associated with MUA recorded on the microelectrodes. (J,K) Examples of a seizure in Patient 1 & 2, showing seizure onset at deep electrode contact and microelectrodes located in periventricular nodules (* on time-axis denotes end of seizure in Patient 1).

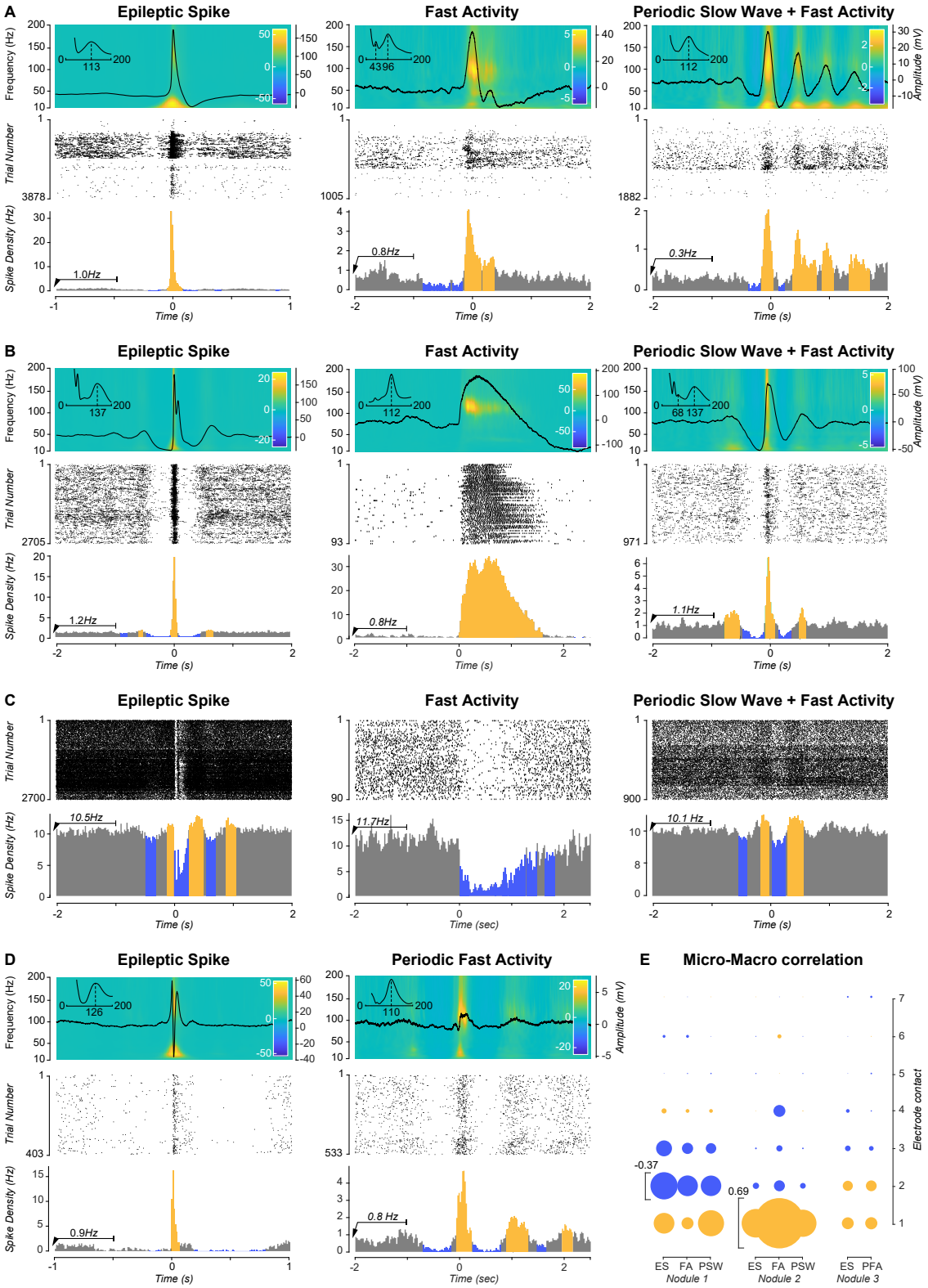

Figure 2: Time-locked LFP and spike analysis (continued on the following page).

Figure 2: Spike analysis shows similarities in pathological patterns between PNH nodules (columns), and involvement of the same neuron in all patterns within nodules (rows). Top row in A-D show average time-locked LFPs of patterns superimposed on average time-resolved spectrum. Middle row in A-D show rasterplots of spike times, time-locked to the patterns. Bottom row in A-D shows corresponding firing-rates, with clusters of significant change (yellow=increase, blue-decrease), compared to baseline (arrow). E) Correlations between micro (LFP) and macro (LFP) contacts (bipolar reference), showing strongest (positive = yellow) correlation with contacts closest to micro electrode (marker-size = Pearson's ρ). Negative correlations (blue) show inversion of dipoles for more superficial macroelectrode contacts. Size of markers scale with ρ.

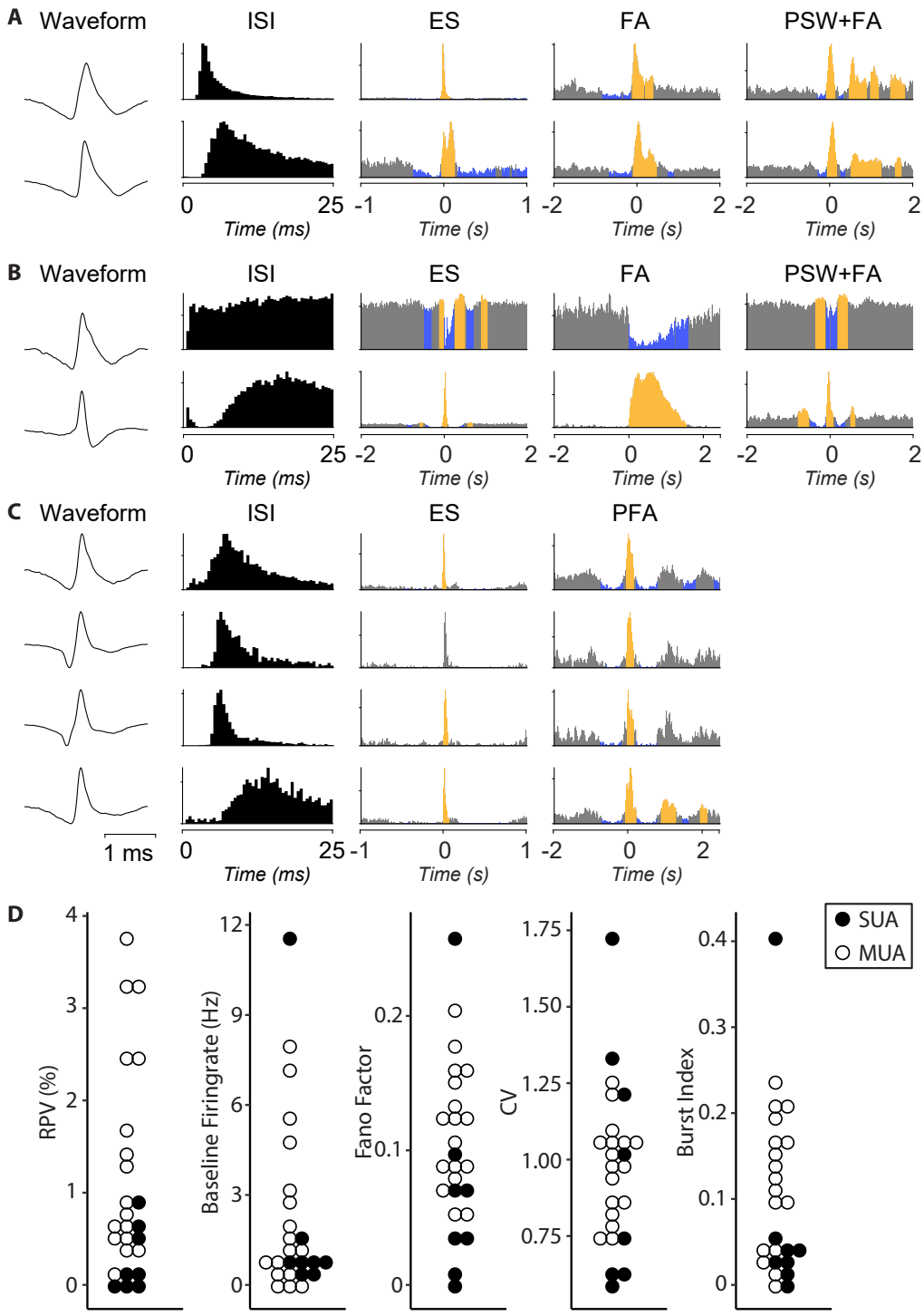

Figure 3: Description of single unit behaviour for Nodule 1 (A), Nodule 2 (B), and Nodule 3 (C), including template waveform, ISI histogram of inter-spike-interval and firing-rates time-locked to epileptic patterns, respectively. Significant increases and decreases in firing-rate compared to baseline are indicated in yellow and blue, respectively. D) Description of unit behaviour, including both SUA (filled), and MUA (empty).

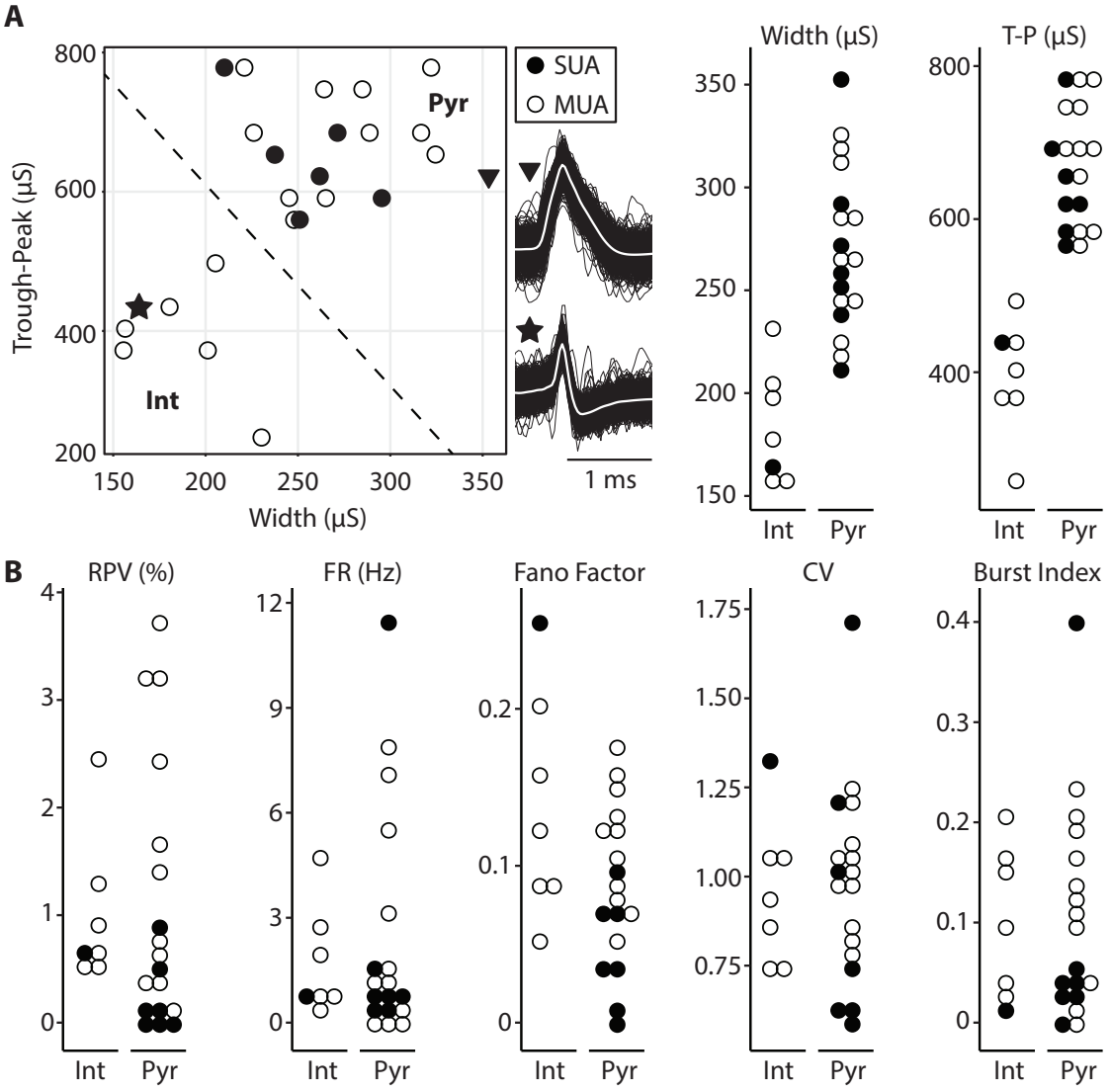

Figure 4: A) Trough to peak plotted against Half-amplitude duration showing two clusters of neuronal types. Pyramidal cells cluster on the top right cluster, interneurons on the bottom-left. Empty symbols indicate putative SUA, filled circus putative MUA. Average waveforms and 1000 overlaid responses show putative pyramidal cell (upside-down pyramid shape), and putative narrow-spiking inter-neuron (star).

Pattern name	Nodule	Filter	Peak	Search period	Baseline period
ES	1	1 : 40	max	-0.1 : 0.1	-1.0 : -0.1
	2	1 : 40	max	-0.1 : 0.2	-1.0 : -0.2
	3	<50	min	-0.025 : 0.05	-0.2 : -0.1
FA	1	1 : 4	first	-0.1 : 0.3	-1.0 : -0.1
	2	1 : 4	first	-0.1 : 1.0	-1.0 : -0.1
PSW	1	1 : 4	max	-0.1 : 0.4	*none*
	2	<4	first	-0.1 : 0.4	-1.0 : -0.1
PFA	3	5 : 50*	max	-0.1 : 0.8	-1.0 : -0.1

Table S1: Parameters of automatic alignment of manually selected patterns

References

Aghakhani, Y. (2005, January). The role of periventricular nodular heterotopia in epileptogenesis. *Brain*, *128*(3), 641–651. Retrieved 2018-05-04, from `https://academic.oup.com/brain/article-lookup/doi/10.1093/brain/awh388` doi: 10.1093/brain/awh388

Alvarado-Rojas, C., Lehongre, K., Bagdasaryan, J., Bragin, A., Staba, R., Engel, J., ... Le Van Quyen, M. (2013). Single-unit activities during epileptic discharges in the human hippocampal formation. *Frontiers in Computational Neuroscience*, *7*, 140. doi: 10.3389/fncom.2013.00140

Barthó, P., Hirase, H., Monconduit, L., Zugaro, M., Harris, K. D., & Buzsáki, G. (2004, July). Characterization of Neocortical Principal Cells and Interneurons by Network Interactions and Extracellular Features. *Journal of Neurophysiology*, *92*(1), 600–608. Retrieved 2018-09-26, from `http://www.physiology.org/doi/10.1152/jn.01170.2003` doi: 10.1152/jn.01170.2003

Battaglia, G., Chiapparini, L., Franceschetti, S., Freri, E., Tassi, L., Bassanini, S., ... Granata, T. (2006, January). Periventricular Nodular Heterotopia: Classification, Epileptic History, and Genesis of Epileptic Discharges. *Epilepsia*, *47*(1), 86–97. Retrieved 2018-05-04, from `http://doi.wiley.com/10.1111/j.1528-1167.2006.00374.x` doi: 10.1111/j.1528-1167.2006.00374.x

Buzsáki, G. (2004, May). Large-scale recording of neuronal ensembles. *Nature Neuroscience*, *7*(5), 446–451. Retrieved 2019-04-25, from `http://www.nature.com/articles/nn1233` doi: 10.1038/nn1233

Calcagnotto, M. E., Paredes, M. F., & Baraban, S. C. (2002, September). Heterotopic neurons with altered inhibitory synaptic function in an animal model of malformation-associated epilepsy. *The Journal of Neuroscience: The Official Journal of the Society for Neuroscience*, *22*(17), 7596–7605.

Castro, P. A., Cooper, E. C., Lowenstein, D. H., & Baraban, S. C. (2001, September). Hippocampal heterotopia lack functional Kv4.2 potassium channels in the methylazoxymethanol model of cortical malformations and epilepsy. *The Journal of Neuroscience: The Official Journal of the Society for Neuroscience*, *21*(17), 6626–6634.

Colacitti, C., Sancini, G., DeBiasi, S., Franceschetti, S., Caputi, A., Frassoni, C., ... Battaglia, G. (1999, January). Prenatal methylazoxymethanol treatment in rats produces brain abnormalities with morphological similarities to human developmental brain dysgeneses. *Journal of Neuropathology and Experimental Neurology*, *58*(1), 92–106. doi: 10.1097/00005072-199901000-00010

Constantinidis, C., & Goldman-Rakic, P. S. (2002, December). Correlated Discharges Among Putative Pyramidal Neurons and Interneurons in the Primate Prefrontal Cortex. *Journal of Neurophysiology*, *88*(6), 3487–3497. Retrieved 2019-07-29, from `https://www.physiology.org/doi/full/10.1152/jn.00188.2002` doi: 10.1152/jn.00188.2002

Dubeau, F., Tampieri, D., Lee, N., Andermann, E., Carpenter, S., Leblanc, R., ... Andermann, F. (1995). Periventricular and subcortical nodular heterotopia A study of 33 patients. *Brain*, *118*(5), 1273–1287. Retrieved 2018-05-04, from `https://academic.oup.com/brain/article-lookup/doi/10.1093/brain/118.5.1273` doi: 10.1093/brain/118.5.1273

Fedorov, A., Beichel, R., Kalpathy-Cramer, J., Finet, J., Fillion-Robin, J.-C., Pujol, S., ... Kikinis, R. (2012, November). 3d Slicer as an image computing platform for the Quantitative Imaging Network. *Magnetic Resonance Imaging*, *30*(9), 1323–1341. doi: 10.1016/j.mri.2012.05.001

Finardi, A., Gardoni, F., Bassanini, S., Lasio, G., Cossu, M., Tassi, L., ... Battaglia, G. (2006, September). NMDA receptor composition differs among anatomically diverse malformations of cortical development. *Journal of Neuropathology and Experimental Neurology*, *65*(9), 883–893. doi: 10.1097/01.jnen.0000235117.67558.6d

Francione, S., Kahane, P., Tassi, L., Hoffmann, D., Durisotti, C., Pasquier, B., & Munari, C. (1994, April). Stereo-EEG of interictal and ictal electrical activity of a histologically proved heterotopic gray matter associated with partial epilepsy. *Electroencephalography and Clinical Neurophysiology*, *90*(4), 284–290. Retrieved 2018-05-04, from `http://linkinghub.elsevier.com/retrieve/pii/0013469494901465` doi: 10.1016/0013-4694(94)90146-5

Fried, I., Wilson, C. L., Maidment, N. T., Engel, J., Behnke, E., Fields, T. A., ... Ackerson, L. (1999, October). Cerebral microdialysis combined with single-neuron and electroencephalographic recording in neurosurgical patients. Technical note. *Journal of Neurosurgery*, *91*(4), 697–705. doi: 10.3171/jns.1999.91.4.0697

Gotman, J., & Gloor, P. (1976, November). Automatic recognition and quantification of interictal epileptic activity in the human scalp EEG. *Electroencephalography and Clinical Neurophysiology*, *41*(5), 513–529.

Guerrini, R., & Dobyns, W. B. (2014, July). Malformations of cortical development: clinical features and genetic causes. *The Lancet Neurology*, *13*(7), 710–726. Retrieved 2018-05-04, from `http://linkinghub.elsevier.com/retrieve/pii/S1474442214700407` doi: 10.1016/S1474-4422(14)70040-7

Henze, D. A., Borhegyi, Z., Csicsvari, J., Mamiya, A., Harris, K. D., & Buzsáki, G. (2000, July). Intracellular Features Predicted by Extracellular Recordings in the Hippocampus In Vivo. *Journal of Neurophysiology*, *84*(1), 390–400. Retrieved 2019-04-25, from `http://www.physiology.org/doi/10.1152/jn.2000.84.1.390` doi: 10.1152/jn.2000.84.1.390

Hirsch, L. J., LaRoche, S. M., Gaspard, N., Gerard, E., Svoronos, A., Herman, S. T., ... Drislane, F. W. (2013). American Clinical Neurophysiology Society's Standardized Critical Care EEG Terminology: 2012 version. *Journal of Clinical Neurophysiology*, *30*(1), 27.

Keller, C. J., Truccolo, W., Gale, J. T., Eskandar, E., Thesen, T., Carlson, C., ... Cash, S. S. (2010, June). Heterogeneous neuronal firing patterns during interictal epileptiform discharges in the human cortex. *Brain*, *133*(6), 1668–1681. Retrieved 2019-06-18, from `https://academic.oup.com/brain/article-lookup/doi/10.1093/brain/awq112` doi: 10.1093/brain/awq112

Kitaura, H., Oishi, M., Takei, N., Fu, Y.-J., Hiraishi, T., Fukuda, M., ... Kakita, A. (2012, July). Periventricular nodular heterotopia functionally couples with the overlying hippocampus: Optical Imaging of PVNH. *Epilepsia*, *53*(7), e127–e131. Retrieved 2018-05-04, from `http://doi.wiley.com/10.1111/j.1528-1167.2012.03509.x` doi: 10.1111/j.1528-1167.2012.03509.x

Kothare, S. V., VanLandingham, K., Armon, C., Luther, J. S., Friedman, A., & Radtke, R. A. (1998, December). Seizure onset from periventricular nodular heterotopias: Depth-electrode study. *Neurology*, *51*(6), 1723–1727. Retrieved 2018-06-19, from `http://www.neurology.org/cgi/doi/10.1212/WNL.51.6.1723` doi: 10.1212/WNL.51.6.1723

Le Van Quyen, M., Bragin, A., Staba, R., Crépon, B., Wilson, C. L., & Engel, J. (2008, June). Cell type-specific firing during ripple oscillations in the hippocampal formation of humans. *The Journal of Neuroscience: The Official Journal of the Society for Neuroscience*, *28*(24), 6104–6110. doi: 10.1523/JNEUROSCI.0437-08.2008

Maris, E., & Oostenveld, R. (2007, August). Nonparametric statistical testing of EEG- and MEG-data.

Journal of Neuroscience Methods, *164*(1), 177–190. doi: 10.1016/j.jneumeth.2007.03.024

Meroni, A., Galli, C., Bramerio, M., Tassi, L., Colombo, N., Cossu, M., ... Spreafico, R. (2009, January). Nodular heterotopia: A neuropathological study of 24 patients undergoing surgery for drug-resistant epilepsy. *Epilepsia*, *50*(1), 116–124. Retrieved 2018-10-02, from `http://doi.wiley.com/10.1111/j.1528-1167.2008.01717.x` doi: 10.1111/j.1528-1167.2008.01717.x

Mirandola, L., Mai, R. F., Francione, S., Pelliccia, V., Gozzo, F., Sartori, I., ... Tassi, L. (2017, November). Stereo-EEG: Diagnostic and therapeutic tool for periventricular nodular heterotopia epilepsies. *Epilepsia*, *58*(11), 1962–1971. Retrieved 2018-05-04, from `http://doi.wiley.com/10.1111/epi.13895` doi: 10.1111/epi.13895

Oostenveld, R., Fries, P., Maris, E., & Schoffelen, J.-M. (2011). FieldTrip: Open Source Software for Advanced Analysis of MEG, EEG, and Invasive Electrophysiological Data. *Computational Intelligence and Neuroscience*, *2011*, 1–9. Retrieved 2015-11-12, from `http://www.hindawi.com/journals/cin/2011/156869/` doi: 10.1155/2011/156869

Palmini, A., Gambardella, A., Andermann, F., Dubeau, F., da Costa, J. C., Olivier, A., ... Kim, H.-I. (1995, April). Intrinsic epileptogenicity of human dysplastic cortex as suggested by corticography and surgical results. *Annals of Neurology*, *37*(4), 476–487. Retrieved 2019-04-26, from `http://doi.wiley.com/10.1002/ana.410370410` doi: 10.1002/ana.410370410

Shinomoto, S., Shima, K., & Tanji, J. (2003, December). Differences in spiking patterns among cortical neurons. *Neural Computation*, *15*(12), 2823–2842. doi: 10.1162/089976603322518759

Stefan, H., Nimsky, C., Scheler, G., Rampp, S., Hopfengärtner, R., Hammen, T., ... Romstöck, J. (2007, January). Periventricular nodular heterotopia: A challenge for epilepsy surgery. *Seizure*, *16*(1), 81–86. Retrieved 2019-05-03, from `https://linkinghub.elsevier.com/retrieve/pii/S1059131106001956` doi: 10.1016/j.seizure.2006.10.004

Tassi, L. (2004, December). Electroclinical, MRI and neuropathological study of 10 patients with nodular heterotopia, with surgical outcomes. *Brain*, *128*(2), 321–337. Retrieved 2018-05-04, from `https://academic.oup.com/brain/article-lookup/doi/10.1093/brain/awh357` doi: 10.1093/brain/awh357

Thom, M., Martinian, L., Parnavelas, J. G., & Sisodiya, S. M. (2004, August). Distribution of Cortical Interneurons in Grey Matter Heterotopia in Patients with Epilepsy. *Epilepsia*, *45*(8), 916–923. Retrieved 2018-05-04, from `http://doi.wiley.com/10.1111/j.0013-9580.2004.46603.x` doi: 10.1111/j.0013-9580.2004.46603.x

Valton, L., Guye, M., McGonigal, A., Marquis, P., Wendling, F., Régis, J., ... Bartolomei, F. (2008,

January). Functional interactions in brain networks underlying epileptic seizures in bilateral diffuse periventricular heterotopia. *Clinical Neurophysiology*, *119*(1), 212–223. Retrieved 2019-01-18, from `https://linkinghub.elsevier.com/retrieve/pii/S1388245707005809` doi: bartho

Yger, P., Spampinato, G. L., Esposito, E., Lefebvre, B., Deny, S., Gardella, C., ... Marre, O. (2018, March). A spike sorting toolbox for up to thousands of electrodes validated with ground truth recordings in vitro and in vivo. *eLife*, *7*. Retrieved 2018-04-11, from `https://elifesciences.org/articles/34518` doi: 10.7554/eLife.34518

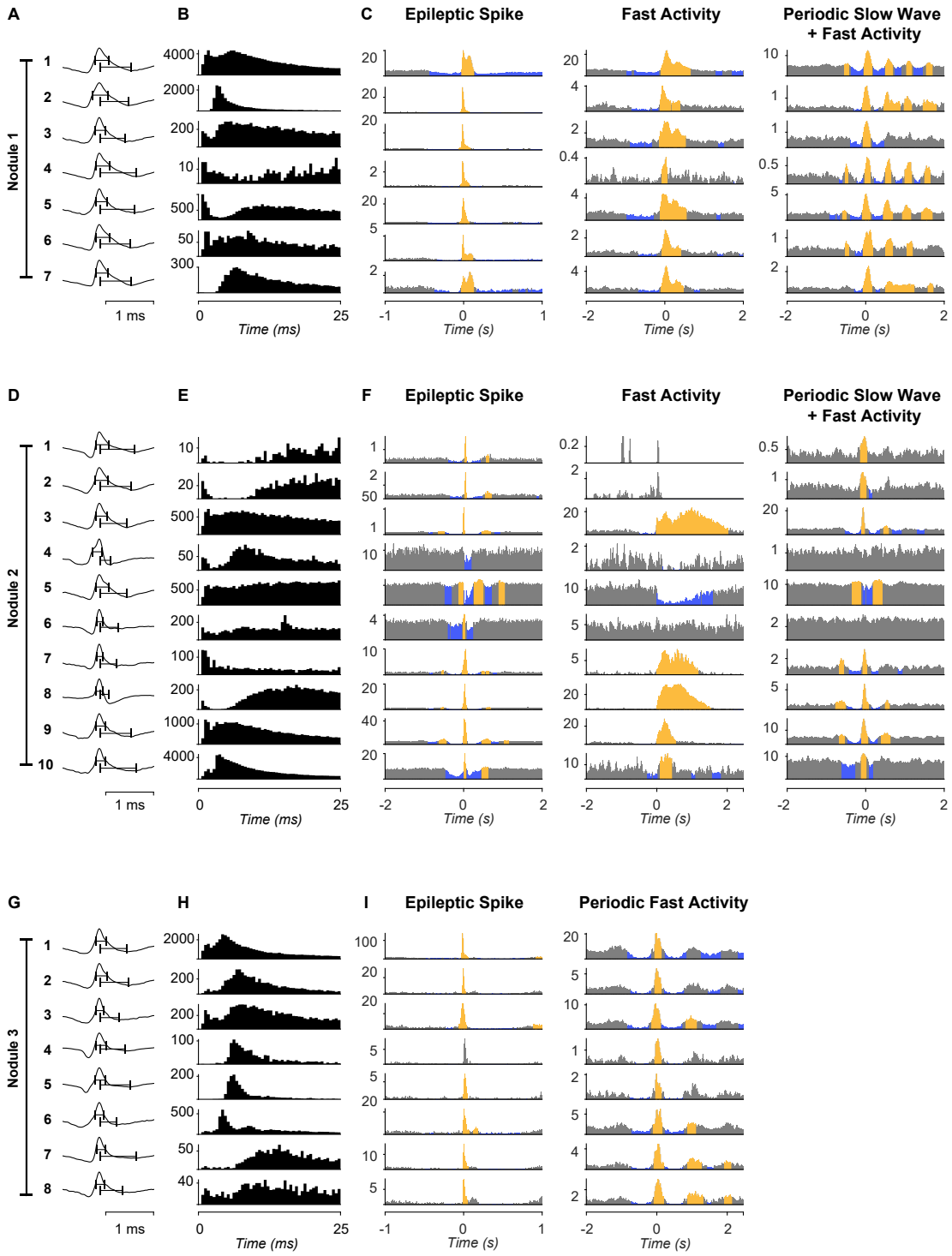

Figure S1: All units